



Cite this: *New J. Chem.*, 2021, 45, 10872

Development of low bandgap polymers for red and near-infrared fullerene-free organic photodetectors†

WonJo Jeong,^{‡,a} Jinhyeon Kang,^{‡,ab} Moon-Ki Jeong,^c Jong Ho Won^b and In Hwan Jung^{id}*^a

Two photoconductive conjugated polymers (PDTPTT and PCPDTTT) were synthesized to be utilized in red and near-infrared (NIR) organic photodetectors (OPDs). The low bandgap was achieved by stabilizing the quinoidal structure of the conjugated backbone, and both donor polymers showed strong red and NIR absorption in the range of 500–900 nm. To enhance the exciton separation and intensify the red and NIR absorption, p–n bulk heterojunction OPDs were fabricated by blending a PDTPTT (or PCPDTTT) and a low bandgap nonfullerene acceptor (IDIC). The PCPDTTT:IDIC devices showed excellent OPD performances with a detectivity (D^*) of 1.14×10^{12} Jones and a –3 dB bandwidth (f_{-3dB}) of 211.7 Hz at –1 V, whereas the PDTPTT:IDIC devices were not successful due to the high dark current density (J_D) at negative bias. The interfacial energies of the PDTPTT:IDIC and PCPDTTT:IDIC blends were calculated by measuring the solvent contact angles and we found that the lower interfacial energy of the PCPDTTT:IDIC blends could make a well-mixed nanomorphology in the blend films, resulting in superior OPD properties. On the other hand, the shallow HOMO energy level (–4.66 eV) of PDTPTT could make substantial J_D , which showed suboptimal OPD performances.

Received 7th April 2021,
Accepted 12th May 2021

DOI: 10.1039/d1nj01694f

rsc.li/njc

Introduction

Polymer-based organic photodetectors (OPDs) have received great attention due to their light weight, solution processability, strong light-absorption coefficient and color tunability of the photoconductive layer.^{1–7} However, due to the strong exciton binding energy of organic materials, the photoconductive layer is commonly required to make bulk heterojunction binary blends composed of a polymer donor and an electron acceptor to increase exciton diffusion and separation.^{8–11} The combination of a donor and an acceptor having different absorption areas makes broad absorption which is the basic strategy to build panchromatic absorption OPDs.^{12–15} On the other hand, matching of the absorption area between a donor and an acceptor

is utilized in color-selective OPDs.^{16,17} Currently, color-selective photoconductive materials for red, green, blue and near-infrared (NIR) OPDs have been developed and several synthetic strategies were reported to increase the responsivity (R) and detectivity (D^*) in the devices.^{18–20} R and D^* are the figures of merit used to evaluate OPD performance. The R is expressed as the photocurrent density (J_{ph}) per input light power (P_{in}), which indicates how many photons are changed into current. However, J_{ph} includes both photocurrent and dark current densities (J_D), and thus R values vary depending on the charge transport mechanism and operating voltage.^{4,21} Thus, D^* considering both the R value and noise spectral density is more important to judge photo-detecting properties.

In the case of blue selective OPDs, high resonance energy benzene rings are commonly introduced in the conjugated backbone not to decrease the bandgap of a polymer donor. However, because it is difficult to make blue selective electron acceptors, Schottky diodes are commonly reported for blue selective OPDs.^{22–24}

In the case of green selective OPDs, the combination of benzene and thiophene rings in the conjugated backbone is highly efficient to make the middle bandgap polymer donor and the representative examples are benzo[1,2-*b*:4,5-*b'*]dithiophene-based polymers.^{16,25} As an acceptor, fullerene derivatives such as [6,6]-phenyl C₇₀ butyric acid methyl ester

^a Department of Organic and Nano Engineering, and Human-Tech Convergence Program, Hanyang University, 222 Wangsimni-ro, Seongdong-gu, Seoul 04763, Republic of Korea. E-mail: inhjung@hanyang.ac.kr

^b Department of Chemistry, Kookmin University, 77 Jeongneung-ro, Seongbuk-gu, Seoul 02707, Republic of Korea

^c School of Chemical and Biological Engineering, Seoul National University, 1 Gwanak-ro, Gwanak-gu, Seoul 08826, Republic of Korea

† Electronic supplementary information (ESI) available: Experimental details, GPC and 1H NMR spectra of the synthesized polymers. See DOI: 10.1039/d1nj01694f

‡ W. Jeong and J. Kang contributed equally to this work.

(PC₇₀BM) are commonly used² and short π -conjugated small-molecule acceptors are recently reported.²⁶

In the case of red selective OPDs, highly π -conjugated backbone structures are required and thus both low bandgap donors and acceptors have been extensively studied. Pecunia *et al.* made p–n bulk heterojunction OPDs composed of a squaraine-based small-molecule donor and a polycyclic aromatic nonfullerene acceptor (NFA). Red selective OPDs were achieved with a D^* of 4.70×10^{11} Jones without any bias and a full width at half maximum (FWHM) of 186 nm. By replacing a donor with a hole transporting polymer, D^* could be increased up to 1.42×10^{13} Jones at 0 V and an FWHM of 141 nm.²⁷ Kim *et al.* developed a diketopyrrolopyrrole-based red polymer, and reported Schottky OPDs with a D^* of 4.63×10^{12} Jones and an FWHM of 148 nm.²⁸ Dong *et al.* reported a squaraine-based small molecule and achieved a D^* of 3.2×10^{12} Jones at -2 V with an FWHM of 80 nm *via* a vacuum-deposited Schottky OPD.²⁹ Luszczynska *et al.* blended a hexafluoroquinoxaline-based donor and an NFA, and reported a D^* of 2×10^{13} Jones at -2 V in the red area.³⁰

In the case of NIR OPDs, broad-band absorption OPDs covering the red and NIR areas have been developed.^{31–33} Nguyen *et al.* developed a cyclopentadithiophene-based small-molecule acceptor and reported a D^* of around 10^{12} Jones at -2 V for the NIR spectral region (up to 1010 nm) by blending with a low bandgap polymer donor.³⁴ Maes *et al.* reported bay-annulated indigo-based NIR absorption copolymers and showed a D^* of 10^{12} Jones at a bias of -2 V within the spectral window of 600–1100 nm.³⁵ Someya *et al.* used an indacenodithiophene-based low bandgap polymer and developed ultra-flexible NIR-responsive OPDs with an outstanding cut-off response frequency over 1 kHz at -3 dB.³⁶ Ng *et al.* developed shortwave infrared OPDs with photoresponse up to 1400 nm, and showed a D^* of around 10^{11} Jones at 0 V.³⁷ Huang *et al.* reported self-filtering narrowband NIR OPDs with an FWHM of ~ 50 nm *via* manipulating the dissociation of Frenkel excitons and showed a high D^* of 1.2×10^{13} Jones at 860 nm under -0.1 V.³⁸

In this study, we developed two low bandgap polymers, poly[(4-(2-ethylhexyl)-4*H*-dithieno[3,2-*b*:2',3'-*d*]pyrrole-2,6-diyl)-*alt*-(2-ethylhexyl-3-fluorothieno[3,4-*b*]thiophene-2-carboxylate 4,6-diyl)] (PDTPTT) and poly[(4,4-bis(2-ethylhexyl)-4*H*-cyclopenta[2,1-*b*:3,4-*b'*]dithiophene-2,6-diyl)-*alt*-(2-ethylhexyl-3-fluorothieno[3,4-*b*]thiophene-2-carboxylate 4,6-diyl)] (PCPDTTT), by Stille coupling of distannylated dithieno[3,2-*b*:2',3'-*d*]pyrrole (DTP) monomer (or distannylated cyclopenta[2,1-*b*:3,4-*b'*]dithiophene (CPDT) monomer) and dibrominated thieno[3,4-*b*]thiophene (TT). DTP^{39–41} and CPDT^{42,43} are well-known strong electron-donating (SD) moieties. The fused ring system of two thiophene rings offers SD properties and the organic soluble alkyl side chains can be introduced at the bridging nitrogen or carbon atom. The resonance effect of the bridging nitrogen makes the DTP ring more electron-donating than the CPDT ring. To make low bandgap polymers, a fluorinated TT ring was copolymerized with DTP or CPDT. TT rings can stabilize the quinoidal structure of the conjugated polymer backbone, which facilitates the bond

length alternation (BLA) of the conjugated ring system.⁴⁴ The reduction of BLA energy indicates a low bandgap polymer.⁴⁵ The synthesized PDTPTT and PCPDTTT donors showed broad absorption in the range of 400–1000 nm, and the maximum absorption peak appeared at around 700 nm. To intensify the red and NIR absorption, a 2,2'-[(4,4,9,9-tetrahexyl-4,9-dihydro-*s*-indaceno[1,2-*b*:5,6-*b'*]dithiophene-2,7-diyl)bis[methylidyne(3-oxo-1*H*-indene-2,1(3*H*)-diylidene)]]bis-propanedinitrile (IDIC) NFA acceptor⁴⁶ was blended with the synthesized donor polymers, and the p–n bulk heterojunction red and NIR photodetectors were successfully developed.

By calculating the interfacial energy between a polymer donor and a NFA acceptor and between organic materials and a processing solvent (chloroform), we found that the low interfacial energy between PDTPTT and CHCl₃ could result in uniform and smooth film surfaces, and the low interfacial energy between PCPDTTT and IDIC could make a well-mixed bulk heterojunction layer with low bimolecular recombination and fast signal response in OPDs. Notably, we suggest that the shallow highest occupied molecular orbital (HOMO) energy level of PDTPTT and the deep lowest unoccupied molecular orbital (LUMO) energy level of IDIC can generate substantial J_D at negative bias, whereas PCPDTTT maintaining a suitable HOMO level was effective to reduce J_D in OPDs. As a result, PCPDTTT:IDIC devices showed promising photodetecting performance with a D^* of 1.14×10^{12} Jones and a -3 dB bandwidth ($f_{-3\text{dB}}$) of 211.7 Hz at -1 V.

Results and discussion

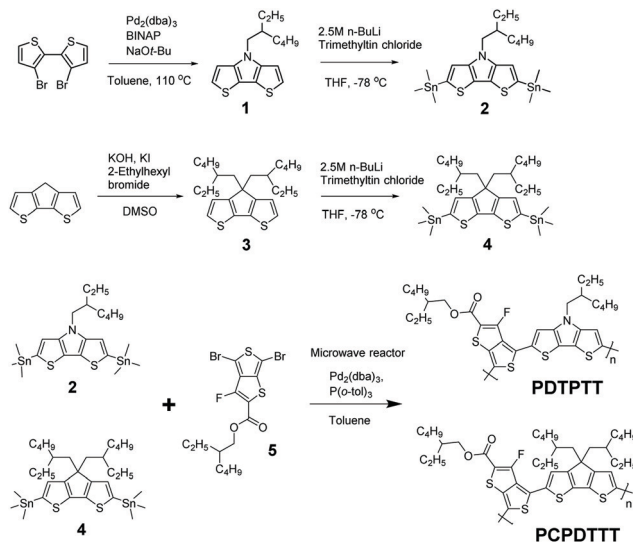
Synthesis and characterization of the polymers

The synthetic route for the PDTPTT and PCPDTTT is shown in Scheme 1. 2-Ethylhexyl 4,6-dibromo-3-fluorothieno[3,4-*b*]thiophene-2-carboxylate (compound 5) was purchased from SunaTech Inc., and 3,3'-dibromo-2,2'-bithiophene and 4*H*-cyclopenta[2,1-*b*:3,4-*b'*]dithiophene were synthesized from the previously reported literature.^{39,43}

Compound 1 was synthesized by the Buchwald–Hartwig amination of 3,3'-dibromo-2,2'-bithiophene and 2-ethylhexylamine, and compound 3 was obtained by the substitution of two 2-ethylhexyl side chains on 4*H*-cyclopenta[2,1-*b*:3,4-*b'*]dithiophene. The final monomers 2 and 4 were synthesized from compound 1 and compound 3, respectively, by the continuous process of lithiation using BuLi and distannylation using trimethyltin chloride. The synthesized monomers were used directly for polymerization.

PDTPTT and PCPDTTT were obtained by microwave-assisted Stille polycondensation of compounds 2 and 5, and compounds 4 and 5, respectively. Both polymers exhibited good solubility in tetrahydrofuran (THF), dichloromethane, chloroform, *etc.*

The number average molecular weight (\overline{M}_n) of polymers was determined by gel permeation chromatography (GPC), and those of PDTPTT and PCPDTTT were 4 kDa ($\overline{D} = 1.2$) and 6.2 kDa ($\overline{D} = 1.4$), respectively. We tried to increase the molecular weight of the polymers using a microwave reactor,



Scheme 1 Synthetic route for poly[(4-(2-ethylhexyl)-4H-dithieno[3,2-*b*:2',3'-*d*]pyrrole-2,6-diyl)-*alt*-(2-ethylhexyl-3-fluorothieno[3,4-*b*]thiophene-2-carboxylate 4,6-diyl)] (PDTPTT) and poly[(4,4-bis(2-ethylhexyl)-4H-cyclopental[2,1-*b*:3,4-*b'*]dithiophene-2,6-diyl)-*alt*-(2-ethylhexyl-3-fluorothieno[3,4-*b*]thiophene-2-carboxylate 4,6-diyl)] (PCPDTTT).

but it was not successful probably due to the impurity in the distannylated monomers 2 and 4. However, both polymer solutions make viscous flows and thus we could obtain uniform and well-coated polymer films enough for the study on the photodetecting properties. The ^1H NMR spectra of the monomers and polymers and GPC spectra were recorded and are shown in the ESI[†] (Fig. S1–S6).

The UV-vis absorption spectra of PDTPTT and PCPDTTT in solution and film were recorded and are shown in Fig. 1a. Both polymers showed strong red and NIR absorption in the range of 550–900 nm. The maximum absorption peak of PDTPTT and PCPDTTT was 667 and 660 nm, respectively, in chloroform, and 678 and 696 nm, respectively, in film. PCPDTTT showed a blue-shifted absorption peak compared to PDTPTT in solution, but the absorption peak of PCPDTTT was strongly red-shifted in

film states, and thus both polymers have similar absorption patterns in film states. The optical bandgaps of PDTPTT and PCPDTTT were estimated from the absorption onset wavelengths (λ_{onset}) of 975 nm and 940 nm, respectively, in film states, and the corresponding bandgaps were 1.27 eV and 1.32 eV, respectively. The bandgap of PDTPTT was lower than that of PCPDTTT, which is because the DTP moiety in PDTPTT has stronger electron-donating properties than the CPDT unit in PCPDTTT.

The HOMO and LUMO energy levels of the polymers were estimated from cyclic voltammetry and shown in Fig. 1b.⁴⁷ The oxidation onset potentials of PDTPTT and PCPDTTT were -0.07 and 0.40 V, respectively, which correspond to -4.66 eV and -5.14 eV, respectively. The shallow HOMO energy level of PDTPTT indicates its strong electron-donating characteristics. The reduction onset potentials of PDTPTT and PCPDTTT similarly appeared near -1.2 V, which correspond to -3.5 eV. The identical electron-withdrawing TT moieties on both polymers resulted in similar LUMO energy levels. As a result, the electron-donating properties of DTP and CPDT cores greatly contributed to the determination of the HOMO energy levels of the polymers, whereas the electron-withdrawing TT moiety contributed to the determination of the LUMO energy levels of the polymers.⁴⁸ The energy level diagram is described in Fig. 1c, and the optical and electrochemical properties are summarized in Table 1.

Photodetecting properties

Bulk heterojunction OPDs were fabricated with a device structure of ITO/ZnO/PEIE/PDTPTT:IDIC or PCPDTTT:IDIC/MoO_x/Ag (Fig. 2a). A collimated 680 nm red LED (Thorlabs, M680L4) was used as a light source and the OPD properties were measured as a function of light intensity. The current density–voltage (*J*-*V*) characteristics of the PDTPTT:IDIC and PCPDTTT:IDIC devices are shown in Fig. 2b and c. Because OPDs require fast response time to be utilized in image sensors, we studied their OPD properties in the photoconductive mode (-1 V and -2 V) which are summarized in Table 2.

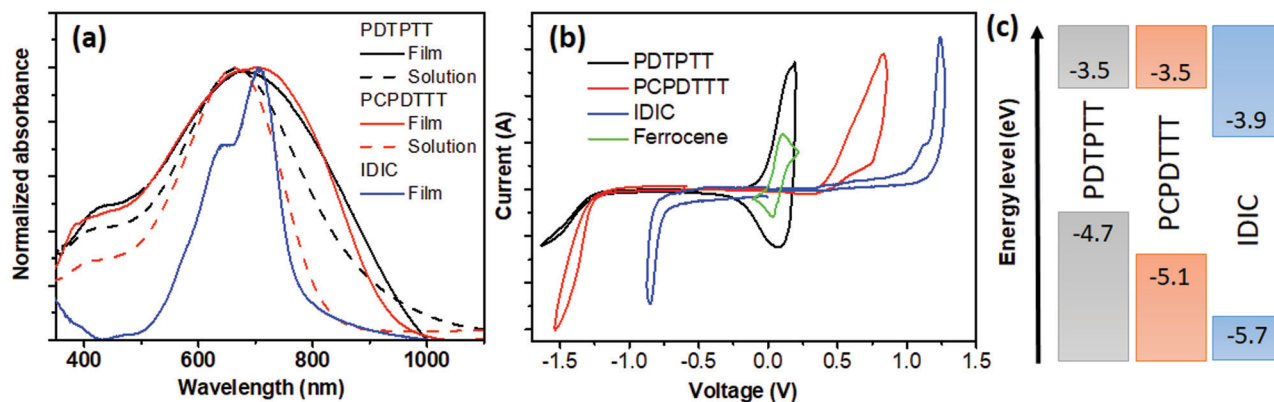


Fig. 1 (a) Absorption spectra of PDTPTT (black line) and PCPDTTT (red line) in solution (dotted line) and film (solid line); the blue line indicates IDIC absorption. (b) Cyclic voltammogram of PDTPTT, PCPDTTT, IDIC and ferrocene; the green line indicates ferrocene reference (the halfway potential ($E^{1/2}$) between ferrocenium (Fc⁺) and ferrocene (Fc) peaks is estimated to be -4.8 eV). (c) Energy level diagram of PDTPTT, PCPDTTT and IDIC.

Table 1 Optical and electrochemical properties of the synthesized PDTPTT and PCPDTTT

	λ_{\max} (nm)		E_{ox} (V)/ $E_{\text{HOMO}}^{\text{CV}}$ (eV) ^c	E_{re} (V)/ $E_{\text{LUMO}}^{\text{CV}}$ (eV) ^d	E_{g}^{CV} (eV) ^e
	Solution ^a	Film ^b			
PDTPTT	667	678	-0.07/-4.66	-1.25/-3.48	1.22
PCPDTTT	660	696	0.40/-5.14	-1.26/-3.47	1.63
IDIC	—	707	0.99/-5.72	-0.81/-3.92	1.78

^a Maximum absorption in chloroform solution. ^b Maximum absorption in film states fabricated by spin-coating of polymer solution. ^c Oxidation potential (E_{ox}) and the corresponding HOMO energy level. ^d Reduction potential (E_{re}) and the corresponding LUMO energy level. ^e Electrochemical bandgap from CV measurement.

The ratio between J_{ph} and J_{D} is called the on/off ratio ($J_{\text{ph}}/J_{\text{D}}$), which is one of the most important parameters to determine photodetecting properties. As shown in Fig. 2b and c, and Table 2, the on/off ratios of PDTPTT:IDIC and PCPDTTT:IDIC devices were 3.88 and 3.56×10^3 , respectively, at -2 V under the light irradiation of 5 mW cm^{-2} . The PCPDTTT:IDIC device showed 1000 times higher on/off ratio than the PDTPTT:IDIC device, indicating superior photodetecting properties of the PCPDTTT:IDIC device.

Responsivity (R) indicates how efficiently photons are changed into current density in the devices, and was calculated from the J_{ph} per P_{in} (Table 2). The R value of the PDTPTT:IDIC device was 0.192 A W^{-1} at -2 V under 5 mW cm^{-2} light power, but its value was significantly increased as the LED power density was decreased. As a result, the R value of the PDTPTT:IDIC device reached 2.44 A W^{-1} at -2 V under 0.010 mW cm^{-2} . However, its high R value was not obtained from the photocurrent density, but mostly from the J_{D} in OPDs. Thus, we could understand that evaluating the device performance by R alone was meaningless. In the case of PCPDTTT:IDIC devices, the R values were relatively constant depending on the light intensity: 90 mA W^{-1} at a light intensity of 0.1 mW cm^{-2} and 64 mA W^{-1} at 5 mW cm^{-2} . Thus, we suggest that R values of OPDs are only reliable when the on/off ratio differed by more than 100.

Notably, the J_{D} values of the PCPDTTT:IDIC devices were effectively suppressed in the photoconductive mode, whereas those of the PDTPTT:IDIC devices were not suppressed. Thus, the comparison of D^* between PCPDTTT:IDIC and

PDTPTT:IDIC devices was more realistic to judge the OPD properties. D^* is expressed as eqn (1), and determined by the noise spectral density and R value of the devices.

$$D^* = \frac{\sqrt{A\Delta f}}{NEP} = \frac{R}{\sqrt{2qJ_{\text{D}}}} [\text{cmHz}^{0.5} \text{ W}^{-1}, \text{jones}] \quad (1)$$

Due to the low J_{D} values of the PCPDTTT:IDIC devices, the D^* values of the PCPDTTT:IDIC devices were at least 10 times higher than those of the PDTPTT:IDIC devices (Table 2). In addition, as shown in Fig. 3a, the D^* values of the PCPDTTT:IDIC devices were much higher than those of the PDTPTT:IDIC devices at all the wavelength area, and the maximum D^* value of the PCPDTTT:IDIC device at 710 nm was 20 times higher than that of the PDTPTT:IDIC device.

The -3 dB bandwidth ($f_{-3\text{dB}}$) was obtained by confirming the frequency response which corresponds to -3 dB from the initial value at -1 V of the bias voltage as shown in Fig. 3b. The $f_{-3\text{dB}}$ was 100.3 Hz for the PDTPTT:IDIC devices and 211.7 Hz for the PCPDTTT:IDIC devices, which implied that the PCPDTTT:IDIC devices had a faster signal response than the PDTPTT devices. As a result, both the static and dynamic properties of the PCPDTTT:IDIC devices were superior to those of the PDTPTT:IDIC devices.

Morphological and charge transport characteristics

The high J_{D} of the PDTPTT:IDIC devices at negative bias was closely related to the energy level difference between the HOMO energy level of the donor ($E_{\text{HOMO,D}}$) and the LUMO energy level of the acceptor ($E_{\text{LUMO,A}}$).⁴⁹ The low energy gap ($E_{\text{HOMO,D}} - E_{\text{LUMO,A}}$) can generate electrical conductivity in the p-n junction diode,⁴⁹ which makes J_{D} in the devices. In our study, PDTPTT had a shallow HOMO energy level of -4.66 eV, which was 0.48 eV higher than that of PCPDTTT (-5.14 eV). As shown in Fig. 2b and 3c, J_{D} of PDTPTT was significantly increased depending on the negative bias and was dominant at low light irradiation. This indicates the induced electric conductivity by applying for the negative bias. On the other hand, PCPDTTT had a much deeper HOMO energy level and a larger energy gap ($E_{\text{HOMO,D}} - E_{\text{LUMO,A}}$) of 1.2 eV than PDTPTT, thus it was more difficult to make J_{D} in the PCPDTTT:IDIC devices. As shown in Fig. 3c, the low J_{D} of the

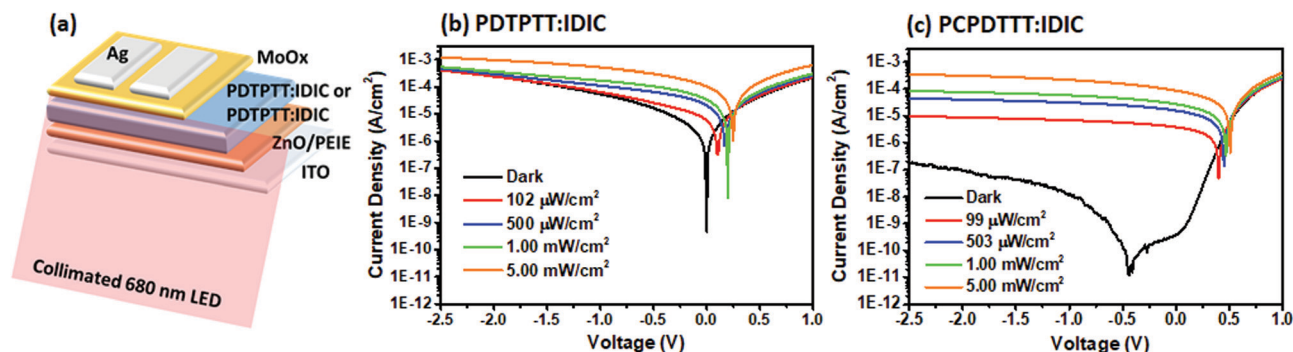


Fig. 2 (a) OPD structures prepared using ITO/ZnO/PEIE/photoconductive layer/MoO_x/Ag. J - V characteristics of the (b) PDTPTT:IDIC and (c) PCPDTTT:IDIC devices as a function of flux under collimated 680 nm red LED illumination.

Table 2 Summary of the photodetecting properties of PDTPTT:IDIC and PCPDTTT:IDIC devices

	Bias (V)	P_{in} ($W\ cm^{-2}$)	J_D ($A\ cm^{-2}$)	J_{ph} ($A\ cm^{-2}$)	On/off ratio	R ($A\ W^{-1}$)	D^* (Jones)
PDTPTT:IDIC	-2	1.02×10^{-4}	2.48×10^{-4}	2.48×10^{-4}	1.00	2.44	2.73×10^{11}
		5.00×10^{-4}	2.48×10^{-4}	2.94×10^{-4}	1.19	5.89×10^{-1}	6.61×10^{10}
		1.00×10^{-3}	2.48×10^{-4}	3.65×10^{-4}	1.47	3.65×10^{-1}	4.10×10^{10}
		5.00×10^{-3}	2.48×10^{-4}	9.62×10^{-4}	3.88	1.92×10^{-1}	2.16×10^{10}
PCPDTTT:IDIC	-2	9.9×10^{-5}	8.95×10^{-8}	8.92×10^{-6}	9.97×10	9.01×10^{-2}	5.32×10^{11}
		5.03×10^{-4}	8.95×10^{-8}	4.11×10^{-5}	4.59×10^2	8.17×10^{-2}	4.83×10^{11}
		1.00×10^{-3}	8.95×10^{-8}	7.76×10^{-5}	8.67×10^2	7.76×10^{-2}	4.58×10^{11}
		5.00×10^{-3}	8.95×10^{-8}	3.19×10^{-4}	3.56×10^3	6.37×10^{-2}	3.77×10^{11}
PDTPTT:IDIC	-1	1.02×10^{-4}	5.48×10^{-5}	6.49×10^{-5}	1.19	6.37×10^{-1}	1.52×10^{11}
		5.00×10^{-4}	5.48×10^{-5}	1.11×10^{-4}	2.03	2.22×10^{-1}	5.31×10^{10}
		1.00×10^{-3}	5.48×10^{-5}	1.72×10^{-4}	3.13	1.72×10^{-1}	4.10×10^{10}
		5.00×10^{-3}	5.48×10^{-5}	5.17×10^{-4}	9.44	1.03×10^{-1}	2.47×10^{10}
PCPDTTT:IDIC	-1	9.9×10^{-5}	1.17×10^{-8}	6.92×10^{-6}	5.93×10^2	6.99×10^{-2}	1.14×10^{12}
		5.03×10^{-4}	1.17×10^{-8}	3.15×10^{-5}	2.70×10^3	6.27×10^{-2}	1.03×10^{12}
		1.00×10^{-3}	1.17×10^{-8}	5.85×10^{-5}	5.01×10^3	5.85×10^{-2}	9.57×10^{11}
		5.00×10^{-3}	1.17×10^{-8}	2.22×10^{-4}	1.90×10^4	4.43×10^{-2}	7.25×10^{11}

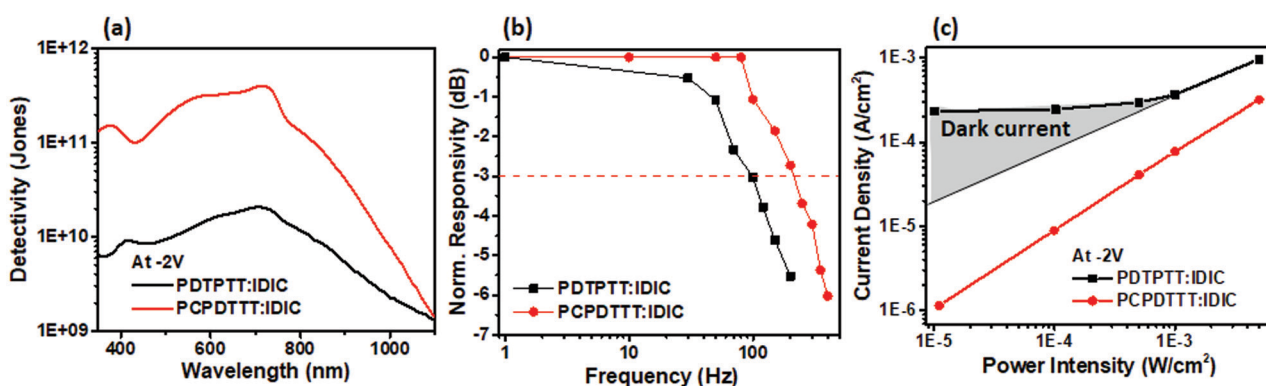


Fig. 3 (a) Detectivity of PDTPTT:IDIC and PCPDTTT:IDIC devices at a bias of -2.0 V as a function of wavelength. (b) The frequency response curve of OPDs at a bias of -1.0 V. (c) The J_{ph} as a function of light power density under 680 nm collimated red LED illumination at -2 V.

PCPDTTT:IDIC devices was advantageous to detect low power light ($0.010\ mW\ cm^{-2}$) signals. In addition, the excellent linear relationship between P_{in} and J_{ph} ($P_{in} = (J_{ph})^2$, $\alpha = 0.999$) indicates the minimized bimolecular recombination process, facilitating charge transfer and fast signal response in OPDs.^{50–52}

The surface morphologies of the PDTPTT:IDIC and PCPDTTT:IDIC films were evaluated by using atomic force

microscopy (AFM) (Fig. S7, ESI[†]). The root-mean-square roughness (R_q) values of the PDTPTT:IDIC and PCPDTTT:IDIC surfaces were 1.10 and 2.63 nm, respectively. The PDTPTT:IDIC blend film showed a more uniform and smooth film surface than the PCPDTTT:IDIC blend film.

To understand the morphological characteristics of these blended films, the water and isopropyl alcohol contact angles were measured on the pristine PDTPTT, PCPDTTT and IDIC films using the sessile drop method (Fig. 4). From the contact angles, the surface free energies of PDTPTT, PCPDTTT and IDIC were calculated using Young's equation ($\gamma_{LV} \cos \theta = \gamma_{SV} + \gamma_{SL}$)⁵³ and Owens and Wendt's geometric mean equation.⁵⁴

$$\gamma_{SL} = \gamma_{LV} + \gamma_{SV} - 2 \left(\sqrt{\gamma_{LV}^d \gamma_{SV}^d} + \sqrt{\gamma_{LV}^p \gamma_{SV}^p} \right) \quad (2)$$

The contact angles and surface energies of PDTPTT, PCPDTTT and IDIC are summarized in Table S1 (ESI[†]) and Table 3, respectively. Finally, we could obtain the interfacial energies between PDTPTT (or PCPDTTT) and IDIC and between PDTPTT, PCPDTTT or IDIC and a processing solvent (chloroform) using their surface energies. As shown in Table S2 (ESI[†]), the

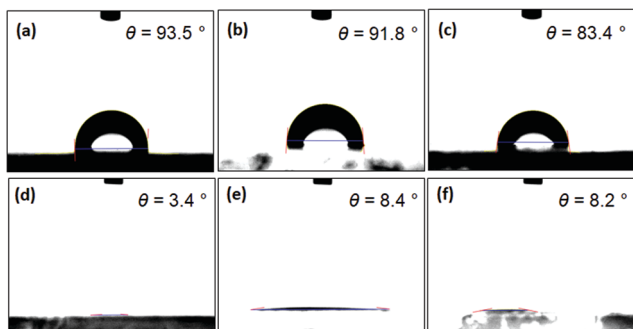


Fig. 4 Wetting angle measurement by water on (a) PDTPTT, (b) PCPDTTT and (c) IDIC films, and by isopropyl alcohol on (d) PDTPTT, (e) PCPDTTT and (f) IDIC films.

Table 3 Calculated dispersive (γ_{sv}^d), polar (γ_{sv}^p) and total (γ_{sv}) surface free energies and polarity of each substance

Surface energy (mJ m^{-2})				
Polymer	γ_{sv}	γ_{sv}^d	γ_{sv}^p	Polarity
PCPDTTT	22.84	18.32	4.52	0.1977
PDTPTT	22.96	19.39	3.57	0.1556
IDIC	24.74	14.78	9.96	0.4026

interfacial energy (1.25 mJ m^{-2}) between PCPDTTT and IDIC was smaller than that (1.91 mJ m^{-2}) between PDTPTT and IDIC. This indicates better mixing in the PCPDTTT:IDIC blend film, which probably resulted in the faster signal response of the PCPDTTT:IDIC devices. On the other hand, the interfacial energy (0.862 mJ m^{-2}) between PDTPTT and chloroform was smaller than that (1.394 mJ m^{-2}) between PCPDTTT and chloroform. Thus, the smooth and uniform surface of the PDTPTT:IDIC blend film would have originated from this low interfacial energy between PDTPTT and chloroform.

Experimental

4-(2-Ethylhexyl)-2,6-bis(trimethylstannyl)-4H-dithieno[3,2-b:2',3'-d']pyrrole (2)

Compound 1 (0.55 g, 1.89 mmol) was dissolved in anhydrous THF (15 mL). 2.5 M *n*-BuLi in hexanes (3.0 mL, 7.50 mmol) was added dropwise to the solution at -78°C and stirred for 2 h. After the solution was stirred 3 h at room temperature, the solution was cooled down to -78°C again, and 1.0 M trimethyltin chloride in THF (10 mL, 10 mmol) was added dropwise and stirred overnight under N_2 atmosphere. The reaction mixture was then extracted with diethyl ether, washed with water, and dried over MgSO_4 . After that, the solvent was removed to afford compound 2 as a brown oil (0.817 g, 70.7%). $^1\text{H-NMR}$ (400 MHz, CDCl_3 , d): 6.96 (s, 2H), 4.06 (m, 2H), 1.98 (br, 1H), 1.31 (m, 8H), 0.90 (t, $J = 6.4$ Hz, 6H), 0.40 (s, 18H)

(4,4-Bis(2-ethylhexyl)-4H-cyclopenta[2,1-b:3,4-b']dithiophene-2,6-diyl)bis(trimethylstannane) (4)

Compound 4 was synthesized with a similar procedure to compound 2. Compound 3 (1.0 g, 2.48 mmol), 2.5 M *n*-BuLi in hexanes (4.0 mL, 10 mmol) and 1.0 M trimethyltin chloride in THF (12.4 mL, 12.4 mmol) were used to afford compound 4 as a brown oil (0.850 g, 47.1%). $^1\text{H-NMR}$ (400 MHz, CDCl_3 , d): 6.94 (s, 2H), 1.83 (m, 4H), 0.98–0.83 (m, 18H), 0.73 (t, $J = 6.4$ Hz, 6H), 0.58 (t, $J = 8.4$ Hz, 6H), 0.36 (s, 18H).

Synthesis of PDTPTT

Compound 2 (200 mg, 0.324 mmol), compound 5 (153 mg, 0.324 mmol), $\text{Pd}_2(\text{dba})_3$ (9 mg, 0.01 mmol) and *p*-(*o*-tolyl) $_3$ (10 mg, 0.03 mmol) were mixed together in a microwave tube. After that, degassed anhydrous toluene (2.0 mL) was added to the mixture. The reaction condition was programmed as follows: 80°C for 10 min, 120°C for 10 min and 150°C for 60 min in a microwave reactor. After polymerization, the

mixture was poured into methanol, and the precipitate was dissolved in chloroform and filtered through Celite to remove the metal catalyst. The polymer fibers were washed by Soxhlet extraction with methanol, acetone and chloroform. The final polymer was obtained after reprecipitation with methanol. PDTPTT: 106.2 mg, 54.3%.

Synthesis of PCPDTTT

PCPDTTT was synthesized with an identical procedure to PDTPTT. Compound 4 (200 mg, 0.275 mmol) and compound 5 (130 mg, 0.275 mmol) were used to obtain the final PCPDTTT (132.0 mg, 67.2%).

Device fabrication

Indium-doped tin oxide-coated glass (ITO-coated glass) was used as the substrate. Each ITO substrate was sonicated for 20 min in acetone, distilled water (D.W), and ethanol. Then, the cleaned ITO-coated glasses were subjected to UV-O_3 treatment for 20 min. The fabricated photodetector was composed of ITO/ZnO/photoconductive layer/ MoO_x/Ag . First, the ZnO layer was used as the electron transporting layer (ETL) *via* a sol-gel process. The precursor solution for the ZnO layer was prepared by dissolving 0.45 M zinc acetate dehydrate ($\text{Zn}(\text{Ac})_2 \cdot \text{H}_2\text{O}$, Alfa Aesar) and 0.45 M ethanolamine ($\text{NH}_2\text{CH}_2\text{CH}_2\text{OH}$, Sigma Aldrich) in 2-methoxyethanol (Alfa Aesar) for 3 h at 60°C . The prepared ZnO precursor solution was spin-coated onto the UV-O_3 -treated ITO substrates at 3000 rpm for 30 s. The ZnO-coated ITO substrates were placed onto a 200°C hot plate and annealed for 10 min. Polyethylene imine (PEIE, Sigma Aldrich, polyethyleneimine, 80% ethoxylated solution, 37 wt% in H_2O) was used for an ETL buffer layer. 0.1 wt% PEIE solution was prepared by diluting the purchased PEIE stock solution in 2-methoxyethanol. Then, the PEIE solution was spin-coated onto the ZnO film at 5000 rpm for 60 sec. After spin-coating, the coated substrates were thermally annealed at 150°C for 10 min. For the photoconductive layer, PCPDTTT and PDTPTT were used as donor materials, and IDIC was used as an acceptor material. Donor and acceptor materials are prepared by stirring with chloroform at a total concentration of 20 mg ml^{-1} for at least 3 hours. At this time, the ratio of the donor and acceptor materials was 1:1 by weight ratio. The blended solution was spin-coated onto the prepared ZnO/ITO substrates. All procedures for the BHJ active layer were carried out in an N_2 -filled glove box. A MoO_x ($\sim 8 \text{ nm}$) layer and an Ag ($\sim 120 \text{ nm}$) layer were deposited by thermal evaporation under a vacuum of $\sim 10^{-6}$ Torr for the hole transporting layer (HTL) and electrode, respectively. The calculated active layer was 0.0707 cm^2 .

Conclusions

PDTPTT and PCPDTTT, two low bandgap polymers, were synthesized *via* the Stille coupling of distannylated DTP or CPDT monomer and dibrominated TT comonomer, respectively. Both donor polymers showed strong red and NIR absorption in the range of 500–900 nm, and a good spectral overlap with an

IDIC acceptor. p–n bulk heterojunction OPDs composed of PDTPTT:IDIC and PCPDTTT:IDIC blend films were fabricated, and the PCPDTTT:IDIC devices showed superior photodetecting properties with a D^* of 1.14×10^{12} Jones and an $f_{-3\text{dB}}$ of 211.7 Hz at -3 dB at -1 V compared to those of the PDTPTT:IDIC devices ($D^* = 1.52 \times 10^{11}$ Jones, $f_{-3\text{dB}} = 100.3$ Hz). By measurement of water and isopropyl alcohol contact angles on the PDTPTT, PCPDTTT and IDIC films, their interfacial energies were calculated and we found that PCPDTTT and IDIC can make better mixing in blend films. In addition, the shallow HOMO energy level (-4.66 eV) of PDTPTT could make substantial dark current density, which resulted in a poor on/off ratio ($J_{\text{ph}}/J_{\text{D}}$) and low D^* in OPDs.

Author contributions

Prof. I. H. Jung planned and supervised this study. W. Jeong and M.-K. Jeong synthesized monomers and polymers. W. Jeong characterized all the materials. J. Kang fabricated and analyzed the OPDs. Prof. J. H. Won studied the surface energy and miscibility of the materials. Prof. I. H. Jung, W. Jeong, and J. Kang wrote the manuscript.

Conflicts of interest

There are no conflicts to declare.

Acknowledgements

This study was supported by the National Research Foundation of Korea (2016R1A5A1012966, 2019R1A2C1089081 and 2020M3H4A3081816). We appreciate Prof. Dae Sung Chung and Ms Juhee Kim from the Pohang University of Science and Technology for studying the dynamic characteristics of OPDs.

References

- 1 F. P. García de Arquer, A. Armin, P. Meredith and E. H. Sargent, *Nat. Rev. Mater.*, 2017, **2**, 16100.
- 2 G. Simone, M. J. Dyson, S. C. J. Meskers, R. A. J. Janssen and G. H. Gelinck, *Adv. Funct. Mater.*, 2020, **30**, 1904205.
- 3 Z. Wu, Y. Zhai, H. Kim, J. D. Azoulay and T. N. Ng, *Acc. Chem. Res.*, 2018, **51**, 3144–3153.
- 4 Y.-L. Wu, K. Fukuda, T. Yokota and T. Someya, *Adv. Mater.*, 2019, **31**, 1903687.
- 5 B. Siegmund, A. Mischok, J. Benduhn, O. Zeika, S. Ullbrich, F. Nehm, M. Böhm, D. Spoltore, H. Fröb, C. Körner, K. Leo and K. Vandewal, *Nat. Commun.*, 2017, **8**, 15421.
- 6 Z. Tang, Z. Ma, A. Sánchez-Díaz, S. Ullbrich, Y. Liu, B. Siegmund, A. Mischok, K. Leo, M. Campoy-Quiles and W. Li, *Adv. Mater.*, 2017, **29**, 1702184.
- 7 T. Li, Z. Chen, Y. Wang, J. Tu, X. Deng, Q. Li and Z. Li, *ACS Appl. Mater. Interfaces*, 2020, **12**, 3301–3326.
- 8 L. Zhu, Y. Yi and Z. Wei, *J. Phys. Chem. C*, 2018, **122**, 22309–22316.
- 9 P. T. van Duijnen, H. D. de Gier, R. Broer and R. W. A. Havenith, *Chem. Phys. Lett.*, 2014, **615**, 83–88.
- 10 S. Few, J. M. Frost and J. Nelson, *Phys. Chem. Chem. Phys.*, 2015, **17**, 2311–2325.
- 11 Z. Liu, X. Chen, S. Huang, H. Guo, F. Wu, J. Wang, J. Liu, X. Huang, L. Chen and Y. Chen, *Chem. Eng. J.*, 2021, **419**, 129532.
- 12 Z. Su, F. Hou, X. Wang, Y. Gao, F. Jin, G. Zhang, Y. Li, L. Zhang, B. Chu and W. Li, *ACS Appl. Mater. Interfaces*, 2015, **7**, 2529–2534.
- 13 P. Sen, R. Yang, J. J. Rech, Y. Feng, C. H. Y. Ho, J. Huang, F. So, R. J. Kline, W. You, M. W. Kudenov and B. T. O'Connor, *Adv. Opt. Mater.*, 2019, **7**, 1801346.
- 14 Y. Han, X. Zhang, F. Zhang, D. Zhao and J. Yu, *Org. Electron.*, 2019, **75**, 105410.
- 15 J. Qi, J. Han, X. Zhou, D. Yang, J. Zhang, W. Qiao, D. Ma and Z. Y. Wang, *Macromolecules*, 2015, **48**, 3941–3948.
- 16 J. Kang, J. Kim, H. Ham, H. Ahn, S. Y. Lim, H. M. Kim, I.-N. Kang and I. H. Jung, *Adv. Opt. Mater.*, 2020, **8**, 2001038.
- 17 S.-J. Lim, D.-S. Leem, K.-B. Park, K.-S. Kim, S. Sul, K. Na, G. H. Lee, C.-J. Heo, K.-H. Lee, X. Bulliard, R.-I. Satoh, T. Yagi, T. Ro, D. Im, J. Jung, M. Lee, T.-Y. Lee, M. G. Han, Y. W. Jin and S. Lee, *Sci. Rep.*, 2015, **5**, 7708.
- 18 R. D. Jansen-van Vuuren, A. Armin, A. K. Pandey, P. L. Burn and P. Meredith, *Adv. Mater.*, 2016, **28**, 4766–4802.
- 19 K. M. Sim, S. Yoon, S.-K. Kim, H. Ko, S. Z. Hassan and D. S. Chung, *ACS Nano*, 2019, **14**, 415–421.
- 20 H. Ren, J.-D. Chen, Y.-Q. Li and J.-X. Tang, *Adv. Sci.*, 2021, **8**, 2002418.
- 21 D. Yang and D. Ma, *Adv. Opt. Mater.*, 2019, **7**, 1800522.
- 22 H. Guo, Y. Wang, R. Wang, S. Liu, K. Huang, T. Michinobu and G. Dong, *ACS Appl. Mater. Interfaces*, 2019, **11**, 16758–16764.
- 23 S. Yoon, Y.-H. Ha, S.-K. Kwon, Y.-H. Kim and D. S. Chung, *ACS Photonics*, 2018, **5**, 636–641.
- 24 D. Bhat, S. Sahoo, J. Bhattacharyya and D. Ray, *Org. Electron.*, 2020, **87**, 105975.
- 25 J. B. Park, J.-W. Ha, S. C. Yoon, C. Lee, I. H. Jung and D.-H. Hwang, *ACS Appl. Mater. Interfaces*, 2018, **10**, 38294–38301.
- 26 T. Lee, S. Oh, S. Rasool, C. E. Song, D. Kim, S. K. Lee, W. S. Shin and E. Lim, *J. Mater. Chem. A*, 2020, **8**, 10318–10330.
- 27 K. Xia, Y. Li, Y. Wang, L. Portilla and V. Pecunia, *Adv. Opt. Mater.*, 2020, **8**, 1902056.
- 28 S. Z. Hassan, H. J. Cheon, C. Choi, S. Yoon, M. Kang, J. Cho, Y. H. Jang, S.-K. Kwon, D. S. Chung and Y.-H. Kim, *ACS Appl. Mater. Interfaces*, 2019, **11**, 28106–28114.
- 29 W. Li, D. Li, G. Dong, L. Duan, J. Sun, D. Zhang and L. Wang, *Laser Photonics Rev.*, 2016, **10**, 473–480.
- 30 T. Klab, B. Luszczynska, J. Ulanski, Q. Wei, G. Chen and Y. Zou, *Org. Electron.*, 2020, **77**, 105527.
- 31 X. Liu, Y. Lin, Y. Liao, J. Wu and Y. Zheng, *J. Mater. Chem. C*, 2018, **6**, 3499–3513.
- 32 Y. Kubo, T. Shimada, K. Maeda and Y. Hashimoto, *New J. Chem.*, 2020, **44**, 29–37.

- 33 A. Armin, R. D. Jansen-van Vuuren, N. Kopidakis, P. L. Burn and P. Meredith, *Nat. Commun.*, 2015, **6**, 6343.
- 34 J. Huang, J. Lee, J. Vollbrecht, V. V. Brus, A. L. Dixon, D. X. Cao, Z. Zhu, Z. Du, H. Wang, K. Cho, G. C. Bazan and T.-Q. Nguyen, *Adv. Mater.*, 2020, **32**, 1906027.
- 35 F. Verstraeten, S. Gielen, P. Verstappen, J. Kesters, E. Georgitzikis, J. Raymakers, D. Cheyens, P. Malinowski, M. Daenen, L. Lutsen, K. Vandewal and W. Maes, *J. Mater. Chem. C*, 2018, **6**, 11645–11650.
- 36 S. Park, K. Fukuda, M. Wang, C. Lee, T. Yokota, H. Jin, H. Jinno, H. Kimura, P. Zalar, N. Matsuhisa, S. Umezue, G. C. Bazan and T. Someya, *Adv. Mater.*, 2018, **30**, 1802359.
- 37 Z. Wu, Y. Zhai, W. Yao, N. Eedugurala, S. Zhang, L. Huang, X. Gu, J. D. Azoulay and T. N. Ng, *Adv. Funct. Mater.*, 2018, **28**, 1805738.
- 38 B. Xie, R. Xie, K. Zhang, Q. Yin, Z. Hu, G. Yu, F. Huang and Y. Cao, *Nat. Commun.*, 2020, **11**, 2871.
- 39 E. Zhou, M. Nakamura, T. Nishizawa, Y. Zhang, Q. Wei, K. Tajima, C. Yang and K. Hashimoto, *Macromolecules*, 2008, **41**, 8302–8305.
- 40 E. Zhou, J. Cong, K. Tajima and K. Hashimoto, *Chem. Mater.*, 2010, **22**, 4890–4895.
- 41 H. L. T. Mai, N. T. T. Truong, T. Q. Nguyen, B. K. Doan, D. H. Tran, L.-T. T. Nguyen, W. Lee, J. W. Jung, M. H. Hoang, H. P. K. Huynh, C. D. Tran and H. T. Nguyen, *New J. Chem.*, 2020, **44**, 16900–16912.
- 42 J. Peet, J. Y. Kim, N. E. Coates, W. L. Ma, D. Moses, A. J. Heeger and G. C. Bazan, *Nat. Mater.*, 2007, **6**, 497–500.
- 43 I. H. Jung, J. Yu, E. Jeong, J. Kim, S. Kwon, H. Kong, K. Lee, H. Y. Woo and H.-K. Shim, *Chem. – Eur. J.*, 2010, **16**, 3743–3752.
- 44 Y. Liang, Z. Xu, J. Xia, S.-T. Tsai, Y. Wu, G. Li, C. Ray and L. Yu, *Adv. Mater.*, 2010, **22**, E135–E138.
- 45 J. L. Brédas, *J. Chem. Phys.*, 1985, **82**, 3808–3811.
- 46 Y. Lin, F. Zhao, Y. Wu, K. Chen, Y. Xia, G. Li, S. K. K. Prasad, J. Zhu, L. Huo, H. Bin, Z.-G. Zhang, X. Guo, M. Zhang, Y. Sun, F. Gao, Z. Wei, W. Ma, C. Wang, J. Hodgkiss, Z. Bo, O. Inganäs, Y. Li and X. Zhan, *Adv. Mater.*, 2017, **29**, 1604155.
- 47 M.-K. Jeong, K. Lee, J. Kang, J. Jang and I. H. Jung, *New J. Chem.*, 2020, **44**, 9321–9327.
- 48 I. H. Jung, W.-Y. Lo, J. Jang, W. Chen, D. Zhao, E. S. Landry, L. Lu, D. V. Talapin and L. Yu, *Chem. Mater.*, 2014, **26**, 3450–3459.
- 49 K. Xu, H. Sun, T.-P. Ruoko, G. Wang, R. Kroon, N. B. Kolhe, Y. Puttison, X. Liu, D. Fazzi, K. Shibata, C.-Y. Yang, N. Sun, G. Persson, A. B. Yankovich, E. Olsson, H. Yoshida, W. M. Chen, M. Fahlman, M. Kemerink, S. A. Jenekhe, C. Müller, M. Berggren and S. Fabiano, *Nat. Mater.*, 2020, **19**, 738–744.
- 50 J. Kim, J. Kang, Y.-S. Park, H. Ahn, S. H. Eom, S.-Y. Jang and I. H. Jung, *Polym. Chem.*, 2019, **10**, 4314–4321.
- 51 S. R. Cowan, A. Roy and A. J. Heeger, *Phys. Rev. B: Condens. Matter Mater. Phys.*, 2010, **82**, 245207.
- 52 J. Rivnay, S. C. B. Mannsfeld, C. E. Miller, A. Salleo and M. F. Toney, *Chem. Rev.*, 2012, **112**, 5488–5519.
- 53 J. H. Won, S. C. Mun, G. H. Kim, H. M. Jeong and J. K. Kang, *Small*, 2020, **16**, 2001756.
- 54 D. K. Owens and R. C. Wendt, *J. Appl. Polym. Sci.*, 1969, **13**, 1741–1747.